RESEARCH

Analysis of thermoelastic damping in a microbeam following a modified strain gradient theory and the Moore-Gibson-Thompson heat equation

Majid M. Kharnoob[1] · Lidia Castro Cepeda[2] · Edwin Jácome[2] · Santiago Choto[2] · Adeeb Abdulally Abdulhussien Alazbjee[3] · I.B. Sapaev[4,5] · Mohammed Ali Mahmood Hussein[6] · Yaicr Yacin[7] · Ahmed Hussien Radie Alawadi[8] · Ali Alsalamy[9]

Abstract

It has been proven that mechanical elements display size-dependent behavior in structural and thermal fields at microscales. It has also been found that thermoelastic damping (TED) is one of the dominant reasons in confining the quality factor (Q-factor) of such elements. This paper aims to develop a novel formulation for evaluating TED in microbeams by accounting for the size effect on the mechanical and thermal areas via the nonclassical theory of modified strain gradient (MSG) and the non-Fourier heat conduction model of Moore-Gibson-Thompson (MGT). In the first step, the heat equation for beams is derived within the framework of MGT model. Through this equation, the function of temperature fluctuation can be obtained. Then, the constitutive relations of the beam according to MSG theory (MSGT) are extracted. By using the temperature distribution and nonclassical constitutive relations obtained, the maximum amounts of potential and wasted thermal energies during one cycle of beam vibration are calculated. Finally, by placing the value of these energies in the existing relationship for computing the value of TED, an explicit expression for TED is presented. With the aim of clarifying the sensitivity of TED value to the characteristic parameters of MSGT and MGT model, a variety of numerical data are provided. According to the obtained outcomes, the inclusion of size effect in the structural and thermal equations can cause a remarkable difference compared to the classical model. The dependency of TED on some factors like beam thickness and aspect ratio, vibration mode number and material of the beam is also investigated numerically.

Keywords Microbeams · Thermoelastic damping · Small-scale effect · Modified strain gradient theory · Moore-Gibson-Thompson thermoelasticity theory

Nomenclature

x, y and z	Principal directions of Cartesian coordinate system
L, h and b	Length, thickness and width of the microbeam, respectively
I, A and V	Moment of inertia of cross sections, cross-sectional area and total volume of the microbeam, respectively

Extended author information available on the last page of the article

™ Springer

u_x, u_y and u_z	Displacements along the directions x, y and z, respectively
w	Transverse displacement
ε_{ij} and σ_{ij} $(i, j = x, y, z)$	Components of strain tensor $\boldsymbol{\varepsilon}$ and stress tensor $\boldsymbol{\sigma}$, respectively
γ_i and p_i $(i = x, y, z)$	Components of dilatation gradient vector $\boldsymbol{\gamma}$ and their stress conjugates, respectively
$\eta_{ijk}^{(1)}$ and $\tau_{ijk}^{(1)}$ $(i, j, k = x, y, z)$	Components of deviatoric stretch gradient tensor $\boldsymbol{\eta}^{(1)}$ and their stress conjugates, respectively
χ_{ij}^s and m_{ij}^s $(i, j = x, y, z)$	Components of symmetric rotation gradient tensor $\boldsymbol{\chi}^s$ and their stress conjugates, respectively
u_i and ϕ_i $(i = x, y, z)$	Components of the displacement vector $\boldsymbol{u}$ and infinitesimal rotation vector $\boldsymbol{\phi}$, respectively
δ_{ij} $(i, j = x, y, z)$	Components of the Kronecker delta
ε_{mm}	Volumetric strain
σ_{mm}	Trace of stress tensor $\boldsymbol{\sigma}$
E, ν and ρ	Elasticity modulus, the Poisson ratio and mass density, respectively
λ and μ	Bulk modulus and shear modulus, respectively
l_0, l_1 and l_2	Material length scale parameters of MSGT
α, k and c_v	Thermal expansion coefficient, thermal conductivity and specific heat per unit mass, respectively
T, T_0 and θ	Current temperature, ambient temperature and temperature change, respectively
ϑ	Thermal displacement
t	Time
$\boldsymbol{q}$	Heat flux vector
τ and k^*	Phase lag of heat flux and thermal conductivity rate, respectively
χ and Δ_E	Thermal diffusivity and relaxation strength, respectively
ω_n	The nth isothermal frequency of vibration
U and K	Stored strain energy and kinetic energy, respectively
ε_{ij}^{th} $(i, j = x, y, z)$	Thermal strain components
M_T	Thermal moment
ΔU and U_{max}	Wasted thermoelastic energy and peak value of strain energy per cycle of vibration, respectively
Q^{-1}	Inverse of quality factor

1 Introduction

Because of some unrivaled properties, including low cost, great sensitivity and ease of integration, the use of micro-electro-mechanical-systems (MEMS) in advanced engineering equipment has met with wide and increasing acceptance. The mechanical part of these systems is made of fundamental structures such as beams. Microbeam resonators have several applications in various fields and can be used as highly sensitive sensors (Zeng et al. 2022; Zhao et al. 2020), force sensors (Luo et al. 2022), scanning probe in atomic force microscopy (AFM) systems (Shi et al. 2020), mass sensors (Zhang 2023), energy converter in energy harvesting systems (Hassena et al. 2021; Sun et al. 2023), actuators (Zhang et al. 2023; Sun et al. 2023), switches (Peng et al. 2019), temperature and vibration sensors (Yang

et al. 2022), etc. Therefore, the correct modeling of such structures plays an important role in accurately predicting the behavior of these systems. Based on the outcomes of several experiments and numerical simulations, structures with micro/nano scale show size-dependent mechanical behaviors. Given the absence of characteristic lengths in the constitutive relations of the classical theory (CT) of elasticity, this theory cannot justify such behavior in micro/nanostructures. Thus, to lift this restriction of CT, several size-dependent elasticity theories containing length scale parameters were proposed. Mindlin and Tiersten (1962) propounded one of the first nonclassical elasticity theories called the couple stress theory (CST). Yang et al. (2002) made some changes to CST and presented a theory called the modified couple stress theory (MCST) with only one characteristic length. Recently, Malikan and Eremeyev (2023) have propounded a new version of MCST based on the fact that in a micro medium, sub-particles can also rotate in addition to rotating the entire domain. According to their model, for precise modeling of the behavior of microstructures, especially in dynamic problems, it is essential to account for the mass inertia caused by micro-rotations, which is overlooked in CST and MCST. To incorporate the influence of mass inertia into governing equations, by exploiting a dynamic length scale (DLS) parameter in conjunction with the static length scale (SLS) parameter of MCST, they defined a kinetic energy relation comprising micro velocities by integrating the velocity of micro-rotations. Their findings revealed that capturing the effect of mass inertia and employing the DLS parameter is quite necessary in some dynamic conditions. By considering the gradient of the strain in addition to the strain, Mindlin and Eshel (1968) established a theory called strain gradient theory (SGT), which includes five additional higher-order constants in addition to two conventional Lame constants of CT. By applying some modifications to SGT, Lam et al. (2003) developed a theory called the modified strain gradient theory (MSGT), in which the potential energy function is defined in terms of second order deformation gradients (that is dilatation gradient vector, deviatoric stretch and symmetric rotation gradient tensors) in addition to first order deformation gradient (strain tensor). Consequently, in MSGT, the number of nonclassical material constants is reduced from five to three, which is an important step in enabling experimental delineation of strain gradient behavior. In addition to the aforementioned size-dependent theories, other higher-order theories like nonlocal theory (NT) (Eringen 1983) and nonlocal strain gradient theory (NSGT) (Lim et al. 2015) have been proposed to accommodate size effect into the constitutive relations of CT. In the last two decades, many investigations have been conducted to survey size-dependent static and dynamic behavior of miniaturized structures on the basis of MCST (Akbarzadeh Khorshidi 2021; Borjalilou and Asghari 2018; Malikan 2017; Zhang and Li 2020; Mirfatah et al. 2022; Tadi Beni et al. 2020), SGT (Malikan and Eremeyev 2023; Delfani et al. 2020; Mousavi and Paavola 2014), MSGT (Shi et al. 2022; Ghayesh et al. 2013; Akgöz and Civalek 2014; Zeighampour and Beni 2014; Uzun et al. 2023; Ansari et al. 2013), NT (Dastjerdi and Abbasi 2020; Ebrahimi-Mamaghani et al. 2020; Abouelregal et al. 2021; Fang et al. 2020; Potapov 2015) and NSGT (Malikan et al. 2020; Panahi et al. 2023; Malikan et al. 2020a,b; Liu et al. 2021; Malikan et al. 2018; Sarparast et al. 2022; Malikan and Nguyen 2018; Yu et al. 2022; Jalil et al. 2023; Esfahani et al. 2019).

The most famous model suggested for heat conduction in solids is the Fourier model. On account of the experimental observations in some special conditions like micro/nano scale and rapid heating, the Fourier model does not have the ability to properly predict heat conduction in the mentioned conditions. To take into account small-scale effect in space or time, researchers paid attention to the introduction of non-Fourier heat conduction models. By adding a phase lag parameter called relaxation time to the Fourier model, Lord and Shulman (1967) put forward a nonclassical model known as the LS model or single-phase-lag (SPL) model. By accommodating a parameter called thermal displacement into

the Fourier model, Green and Naghdi (1993) presented another non-Fourier model known as GN-III model. In order to benefit from the advantages of both SPL and GN-III models, by merging these two models, a powerful model containing two nonclassical constants called Moore-Gibson-Thompson (MGT) model (Quintanilla 2019) was introduced. In addition to the reviewed non-Fourier models, other nonclassical heat conduction models such as dual-phase-lag (DPL) (Tzou 1995), nonlocal single-phase-lag (NSPL) (Guyer and Krumhansl 1966) and nonlocal dual-phase-lag (NDPL) (Tzou and Guo 2010) models have also been provided to account for the effect of size in space and time.

One of the key factors in the design of resonators consisting of mechanical elements is to minimize the amount of energy loss in order to achieve optimal performance. Based on several empirical findings, thermoelastic damping (TED) is one of the inevitable causes of energy dissipation in structures with micro dimensions. In this type of energy dissipation mechanism, when a mechanical element is subjected to bending, because of the coupling between strain and temperature fields, a temperature distribution is generated across the element. This temperature difference between different points of the structure causes heat flow across it. Since this process is thermodynamically irreversible, the entropy of the system increases and its energy is lost thermally, which is the phenomenon of thermoelastic damping. Two complex frequency (CF) and energy dissipation (ED) approaches are used to calculate the amount of TED in structures by theoretical methods. Zener (1937) applied ED approach for the first time to provide an analytical relation for approximating TED value in Euler-Bernoulli beams. His formulation has been derived in the framework of CT and the Fourier model. Lifshitz and Roukes (2000) conducted a similar study to the investigation of Zener, but within the framework of CF approach.

During the last two decades, various theoretical studies have been done to model TED in basic mechanical elements. Some of the most important investigations on TED in beams are introduced in the following. In the framework of CT and Fourier model, Prabhakar and Vengallatore (2008) utilized Green's function technique to assess TED in microresonators with two-dimensional (2D) heat conduction. Tunvir et al. (2012) studied TED in geometrically nonlinear microbeams by employing CT and Fourier law. According to classical versions of elasticity theory and heat equation, Emami and Alibeigloo (2016) presented an analytical solution for TED in functionally graded (FG) Timoshenko beams. Rezazadeh et al. (2012) conducted a size-dependent analysis on TED in thin beams via MCST and Fourier heat equation. Yu et al. (2017) developed a formulation on the basis of NT and NSPL model to determine the effect of size on TED. Abedi et al. (2023) examined thermal and hydraulic properties of air and water under different operating conditions to evaluate the technology's thermal efficiency and water treatment capacity. With the help of CT and SPL model, Zhou et al. (2018) provided an analytical solution for TED in beams with circular cross section. Gu et al. (2021) carried out an analytical study to examine size effect on TED by means of NSGT and DPL model. In the context of CT and Fourier model, Zuo et al. (2022) established a relation for computing TED value in anisotropic piezoelectric microbeams. Borjalilou et al. (2020) employed NT together with DPL model to survey size-dependent TED in nanobeam resonators. Singh et al. (2021) developed a size-dependent solution for TED in small-sized beams on the basis of MCST and MGT model. In addition to the reviewed studies, other theoretical researches have been performed on TED in various elements such as beams (Tiwari et al. 2022; Borjalilou and Asghari 2019; Kumar et al. 2022, 2018; Borjalilou et al. 2019; Kumar and Mukhopadhyay 2020; Abbas 2016; Kumar 2020, 2021; Kumar and Kumar 2021), plates (Peng et al. 2022; Grover and Seth 2019; Singh et al. 2022; Fredi et al. 2020; Xiao et al. 2021; Yang et al. 2021; Li and Esmaeili 2021), shells (Loghman and Moradi 2013; Li et al. 2022; Atta et al. 2023; Li et al. 2022) and rings (Jalil et al. 2023; Ge and Sarkar 2022; Zhong et al. 2022; Jalil et al. 2023; Kim and Kim 2023).

Given the literature survey performed above, the use of scale-dependent continuum mechanics theories and non-Fourier heat equations is inevitable to precisely anticipate thermomechanical behaviors of microstructures, including thermoelastic damping (TED) phenomenon in microbeam resonators. According to the current available literature, up till now, no theoretical investigation has been published on TED in microbeams via the combination of MSGT and MGT model in the framework of energy dissipation (ED) approach. The paper at hand tries to remove this deficiency from the literature. To attain this purpose, the heat equation of the microbeam is initially derived in the context of MGT model. By solving this partial differential equation (PDE), the function of temperature field is extracted. Then, the scale-dependent constitutive relations of the microbeam are obtained according to MSGT. By making use of the obtained temperature field and strain gradient-based constitutive relations, the highest values of elastic strain and wasted thermal energies per cycle of oscillation can be determined. By putting the relation of these energies in the relationship for TED in ED approach, a closed-form TED expression is presented. To survey the dependency of TED on the specific parameters of MSGT and MGT model, a variety of numerical results are provided.

2 Moore-Gibson-Thompson heat equation

Heat conduction equation within the framework of Moore-Gibson-Thompson (MGT) model is described by the following relation (Quintanilla 2019):

$$\left(1 + \tau \frac{\partial}{\partial t}\right) \boldsymbol{q} = -\left(k \boldsymbol{\nabla} \theta + k^* \boldsymbol{\nabla} \vartheta\right) \tag{1}$$

where the vector symbol $\boldsymbol{\nabla}$ refers to the gradient operator. Variable $\boldsymbol{q}$ denotes heat flux vector. In addition, variable $\theta = T - T_0$ stands for temperature change in which T and T_0 are the current and ambient temperatures, respectively. Variable ϑ is also called thermal displacement, which is related to temperature change θ through the relation $\theta = \partial \vartheta / \partial t$. Parameter τ is known as the phase lag of heat flux. Moreover, material constants k and k^* represent the thermal conductivity and thermal conductivity rate, respectively. Note that when the term containing k^* vanishes, Eq. (1) reduces to the heat equation of LS model. Also, by dropping the term including τ, the formulation of MGT model corresponds to that of GN-III model. In addition, when both k^* and τ are set to zero, Eq. (1) turns into the relation of Fourier law.

Conservation of energy in solids can be expressed via the relation below (Tzou 1995):

$$\boldsymbol{\nabla}.\boldsymbol{q} = -\left(\rho c_v \frac{\partial \theta}{\partial t} + \frac{E \alpha T_0}{1 - 2v} \frac{\partial \varepsilon_{mm}}{\partial t}\right) \tag{2}$$

Here, the variable ε_{mm} represents volumetric strain, which is calculated by the trace of strain tensor $\boldsymbol{\varepsilon}$. Furthermore, ρ and c_v are symbols for mass density and specific heat per unit mass, respectively. Parameter α is also thermal expansion coefficient. Additionally, parameters E and v refer to the elasticity modulus and the Poisson ratio of the material, respectively. If the heat flux $\boldsymbol{q}$ is removed from Eqs. (1) and (2), the MGT-based heat conduction equation in terms of temperature change and strains is obtained as follows:

$$k \frac{\partial}{\partial t}\left(\nabla^2 \theta\right) + k^* \nabla^2 \theta = \left(1 + \tau \frac{\partial}{\partial t}\right)\left(\rho c_v \frac{\partial^2 \theta}{\partial t^2} + \frac{E \alpha T_0}{1 - 2v} \frac{\partial^2 \varepsilon_{mm}}{\partial t^2}\right) \tag{3}$$

where $\nabla^2 = \boldsymbol{\nabla}.\boldsymbol{\nabla}$ defines the Laplace operator.

3 Modified strain gradient theory

On the basis of modified strain gradient theory (MSGT) introduced by Lam et al. (2003), the variation of stored strain energy U in a continuum occupying volume V is given by:

$$\delta U = \iiint_V \left(\sigma_{ij}\delta\varepsilon_{ij} + p_i\delta\gamma_i + \tau_{ijk}^{(1)}\delta\eta_{ijk}^{(1)} + m_{ij}^s\delta\chi_{ij}^s \right) dV \tag{4}$$

in which variables ε_{ij}, γ_i, $\eta_{ijk}^{(1)}$ and χ_{ij}^s represent the components of the strain tensor $\boldsymbol{\varepsilon}$, dilatation gradient vector $\boldsymbol{\gamma}$, deviatoric stretch gradient tensor $\boldsymbol{\eta}^{(1)}$ and symmetric rotation gradient tensor $\boldsymbol{\chi}^s$, respectively. These kinematic variables are computed via the following relations:

$$\varepsilon_{ij} = \frac{1}{2}\left(\frac{\partial u_i}{\partial x_j} + \frac{\partial u_j}{\partial x_i} \right) \tag{5a}$$

$$\gamma_i = \frac{\partial \varepsilon_{mm}}{\partial x_i} \tag{5b}$$

$$\eta_{ijk}^{(1)} = \frac{1}{3}\left(\frac{\partial \varepsilon_{jk}}{\partial x_i} + \frac{\partial \varepsilon_{ki}}{\partial x_j} + \frac{\partial \varepsilon_{ij}}{\partial x_k} \right) - \frac{1}{15}\delta_{ij}\left(\frac{\partial \varepsilon_{mm}}{\partial x_k} + 2\frac{\partial \varepsilon_{mk}}{\partial x_m} \right)$$
$$- \frac{1}{15}\delta_{jk}\left(\frac{\partial \varepsilon_{mm}}{\partial x_i} + 2\frac{\partial \varepsilon_{mi}}{\partial x_m} \right) - \frac{1}{15}\delta_{ki}\left(\frac{\partial \varepsilon_{mm}}{\partial x_j} + 2\frac{\partial \varepsilon_{mj}}{\partial x_m} \right) \tag{5c}$$

$$\chi_{ij}^s = \frac{1}{2}\left(\frac{\partial \phi_i}{\partial x_j} + \frac{\partial \phi_j}{\partial x_i} \right) \quad \text{with} \quad \phi_i = \frac{1}{2}\left(curl\left(\boldsymbol{u} \right) \right)_i \tag{5d}$$

Here, u_i and ϕ_i denote the components of the displacement vector $\boldsymbol{u}$ and infinitesimal rotation vector $\boldsymbol{\phi}$, respectively. Moreover, δ_{ij}, δ_{jk} and δ_{ki} represent the components of the Kronecker delta. Also, parameters σ_{ij}, p_i, $\tau_{ijk}^{(1)}$ and m_{ij}^s appeared in Eq. (4) stand for the stress conjugates of ε_{ij}, γ_i, $\eta_{ijk}^{(1)}$ and χ_{ij}^s, respectively. The classical constitutive relation is expressed as follows:

$$\sigma_{ij} = \lambda\varepsilon_{mm}\delta_{ij} + 2\mu\varepsilon_{ij} - (3\lambda + 2\mu)\alpha\theta\delta_{ij} \tag{6a}$$

Moreover, higher-order constitutive relations based on MSGT are given by (Lam et al. 2003):

$$p_i = 2\mu l_0^2\gamma_i \tag{6b}$$

$$\tau_{ijk}^{(1)} = 2\mu l_1^2\eta_{ijk}^{(1)} \tag{6c}$$

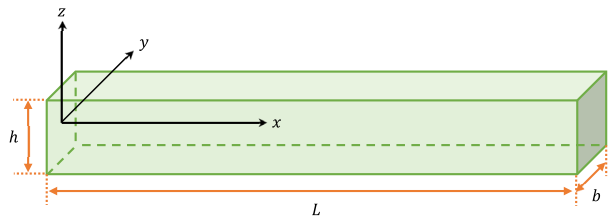$$m_{ij}^s = 2\mu l_2^2\chi_{ij}^s \tag{6d}$$

In the above equations, the coefficients λ and μ address the bulk and shear moduli, respectively, which are defined by:

$$\lambda = \frac{E\nu}{(1+\nu)(1-2\nu)} \tag{7a}$$

$$\mu = \frac{E}{2(1+\nu)} \tag{7b}$$

Fig. 1 Beam configuration and coordinate system

Moreover, l_0, l_1 and l_2 are additional material length scale parameters relevant to dilatation, deviatoric stretch and rotation gradients, respectively. The point to be noted here is that in the case of $l_0 = l_1 = 0$, the equations of MSGT are converted to those of MCST. Furthermore, in the absence of all three characteristic lengths l_0, l_1 and l_2, the relations obtained based on MSGT are reduced to those derived in the framework of CT.

4 Problem formulation

4.1 Coupled thermoelastic constitutive relations of Euler-Bernoulli beams based on MSGT

Geometry and coordinate system of a beam with length L, thickness h and width b are displayed in Fig. 1. The area of cross section and volume of the beam are shown by A and V, respectively.

According to Euler-Bernoulli beam theory, the displacement field of different points of beam is expressed via the following relations:

$$u_x = -z \frac{\partial w(x,t)}{\partial x}, \quad u_y = 0, \quad u_z = w(x,t) \tag{8}$$

Here, u_x, u_y and u_z represent displacements along the directions x, y and z, respectively. Function $w(x,t)$ is also transverse or lateral deflection of the beam. By placing Eq. (8) into Eqs. (5a)-(5d), one can attain the components of kinematic parameters $\boldsymbol{\varepsilon}$, $\boldsymbol{\gamma}$, $\boldsymbol{\eta}^{(1)}$ and $\boldsymbol{\chi}^s$ as follows:

$$\varepsilon_{xx} = -z \frac{\partial^2 w}{\partial x^2} \tag{9a}$$

$$\gamma_x = -z \frac{\partial^3 w}{\partial x^3}, \quad \gamma_z = -\frac{\partial^2 w}{\partial x^2} \tag{9b}$$

$$\eta_{xxx}^{(1)} = -\frac{2}{5} z \frac{\partial^3 w}{\partial x^3}, \quad \eta_{xyy}^{(1)} = \eta_{yxy}^{(1)} = \eta_{yyx}^{(1)} = \frac{1}{5} z \frac{\partial^3 w}{\partial x^3}$$

$$\eta_{xxz}^{(1)} = \eta_{xzx}^{(1)} = \eta_{zxx}^{(1)} = -\frac{4}{15} \frac{\partial^2 w}{\partial x^2}, \quad \eta_{xzz}^{(1)} = \eta_{zxz}^{(1)} = \eta_{zzx}^{(1)} = \frac{1}{5} z \frac{\partial^3 w}{\partial x^3} \tag{9c}$$

$$\eta_{yyz}^{(1)} = \eta_{yzy}^{(1)} = \eta_{zyy}^{(1)} = \frac{1}{15} \frac{\partial^2 w}{\partial x^2}, \quad \eta_{zzz}^{(1)} = \frac{1}{5} \frac{\partial^2 w}{\partial x^2}$$

$$\chi_{xy}^s = \chi_{yx}^s = -\frac{1}{2} \frac{\partial^2 w}{\partial x^2} \tag{9d}$$

By performing mathematical operations in Eq. (6a) and employing Eqs. (7a) and (7b), the strain components can be expressed in terms of stress components as follows:

$$\varepsilon_{ij} = \frac{1}{E}\left[(1+v)\,\sigma_{ij} - v\sigma_{mm}\delta_{ij}\right] + \alpha\theta\delta_{ij} \tag{10}$$

in which σ_{mm} denotes the trace of Cauchy tensor $\boldsymbol{\sigma}$. By assuming the uniaxial state of stress, that is $\sigma_{yy} = \sigma_{zz} = 0$, Eq. (10) yields the following relation:

$$\sigma_{xx} = E\varepsilon_{xx} - E\alpha\theta \tag{11}$$

By substituting Eqs. (9a)-(9d) into Eqs. (6b)-(6d) and (11), one can get:

$$\sigma_{xx} = -Ez\frac{\partial^2 w}{\partial x^2} - E\alpha\theta \tag{12a}$$

$$p_x = -2\mu l_0^2 z\frac{\partial^3 w}{\partial x^3}, \quad p_z = -2\mu l_0^2\frac{\partial^2 w}{\partial x^2} \tag{12b}$$

$$\tau_{xxx}^{(1)} = -\frac{4}{5}\mu l_1^2 z\frac{\partial^3 w}{\partial x^3}, \quad \tau_{xyy}^{(1)} = \tau_{yxy}^{(1)} = \tau_{yyx}^{(1)} = \frac{2}{5}\mu l_1^2 z\frac{\partial^3 w}{\partial x^3}$$

$$\tau_{xxz}^{(1)} = \tau_{xzx}^{(1)} = \tau_{zxx}^{(1)} = -\frac{8}{15}\mu l_1^2\frac{\partial^2 w}{\partial x^2}, \quad \tau_{xzz}^{(1)} = \tau_{zxz}^{(1)} = \tau_{zzx}^{(1)} = \frac{2}{5}\mu l_1^2 z\frac{\partial^3 w}{\partial x^3} \tag{12c}$$

$$\tau_{yyz}^{(1)} = \tau_{yzy}^{(1)} = \tau_{zyy}^{(1)} = \frac{2}{15}\mu l_1^2\frac{\partial^2 w}{\partial x^2}, \quad \tau_{zzz}^{(1)} = \frac{2}{5}\mu l_1^2\frac{\partial^2 w}{\partial x^2}$$

$$m_{xy}^s = m_{yx}^s = -\mu l_2^2\frac{\partial^2 w}{\partial x^2} \tag{12d}$$

By employing Eq. (8) and overlooking the rotary inertia of cross sections of the beam, the variation of the kinetic energy K can be expressed by:

$$\delta K = \iiint\limits_{V}\left[\frac{\partial u_x}{\partial t}\delta\left(\frac{\partial u_x}{\partial t}\right) + \frac{\partial u_y}{\partial t}\delta\left(\frac{\partial u_y}{\partial t}\right) + \frac{\partial u_z}{\partial t}\delta\left(\frac{\partial u_z}{\partial t}\right)\right]\rho dV$$

$$\approx \iiint\limits_{V}\left[\frac{\partial w}{\partial t}\delta\left(\frac{\partial w}{\partial t}\right)\right]\rho dV \tag{13}$$

To derive the governing motion equation and boundary conditions of the beam, Hamilton's principle is exploited as follows:

$$\int_0^t (\delta U - \delta K)dt = 0 \tag{14}$$

By utilizing Eqs. (9a)-(9d) and (12a)-(12d) in Eq. (4), inserting the result together with Eq. (13) into Eq. (14) and implementing the integration by parts, one can arrive at the equation of motion and boundary conditions of the beam as follows:

$$D_1\frac{\partial^6 w}{\partial x^6} - D_2\frac{\partial^4 w}{\partial x^4} - \frac{\partial^2 M_T}{\partial x^2} - \rho A\frac{\partial^2 w}{\partial t^2} = 0 \tag{15}$$

$$\left(D_1 \frac{\partial^5 w}{\partial x^5} - D_2 \frac{\partial^3 w}{\partial x^3} - \frac{\partial M_T}{\partial x} \right) . \delta w = 0 \tag{16a}$$

$$\left(D_1 \frac{\partial^4 w}{\partial x^4} - D_2 \frac{\partial^2 w}{\partial x^2} - M_T \right) . \delta \left(\frac{\partial w}{\partial x} \right) = 0 \tag{16b}$$

$$\left(D_1 \frac{\partial^3 w}{\partial x^3} \right) . \delta \left(\frac{\partial^2 w}{\partial x^2} \right) = 0 \tag{16c}$$

where M_T represents the thermal moment which can be calculated from the following relation:

$$M_T = E\alpha \iint_A \theta z \, dA = E\alpha b \int_{-h/2}^{+h/2} \theta z \, dz \tag{17}$$

Moreover, the nonclassical coefficients D_1 and D_2 are defined by:

$$D_1 = \mu I \left(2l_0^2 + \frac{4}{5} l_1^2 \right) \tag{18a}$$

$$D_2 = EI + \mu A \left(2l_0^2 + \frac{8}{15} l_1^2 + l_2^2 \right) \tag{18b}$$

Here, I refers to the area moment of inertia of sections about y-axis which is expressed by:

$$I = \iint_A z^2 \, dA = b \int_{-h/2}^{+h/2} z^2 \, dz \tag{19}$$

4.2 MGT-based heat equation for Euler-Bernoulli beams

By considering the uniaxial state of stress ($\sigma_{yy} = \sigma_{zz} = 0$) and inserting Eq. (11) into Eq. (10), one can get:

$$\varepsilon_{yy} = \varepsilon_{zz} = \nu z \frac{\partial^2 w}{\partial x^2} + (1 + \nu) \alpha \theta \tag{20}$$

By use of Eqs. (9a) and (20), the following relation for volumetric strain ε_{mm} is obtained:

$$\varepsilon_{mm} = \varepsilon_{xx} + \varepsilon_{yy} + \varepsilon_{zz} = (2\nu - 1) z \frac{\partial^2 w}{\partial x^2} + 2(1 + \nu)\alpha\theta \tag{21}$$

By substituting above equation into Eq. (3) and simplifying the result, the heat equation takes the following form:

$$k \frac{\partial}{\partial t} \left(\nabla^2 \theta \right) + k^* \nabla^2 \theta = \left(1 + \tau \frac{\partial}{\partial t} \right) \left\{ \rho c_v \left[1 + \Delta_E \frac{2(1 + \nu)}{1 - 2\nu} \right] \frac{\partial^2 \theta}{\partial t^2} - E\alpha T_0 z \frac{\partial^4 w}{\partial x^2 \partial t^2} \right\} \tag{22}$$

in which

$$\Delta_E = \frac{E\alpha^2 T_0}{\rho c_v} \tag{23}$$

For most materials, Δ_E takes a very small value, so that $\Delta_E \ll 1$. Consequently, Eq. (22) can be replaced by the simpler equation below:

$$k\frac{\partial}{\partial t}\left(\nabla^2\theta\right) + k^*\nabla^2\theta = \left(1 + \tau\frac{\partial}{\partial t}\right)\left(\rho c_v\frac{\partial^2\theta}{\partial t^2} - E\alpha T_0 z\frac{\partial^4 w}{\partial x^2\partial t^2}\right) \tag{24}$$

To extract the function of temperature change θ from above equation, the following harmonic forms are considered for functions θ and w:

$$\theta(x, z, t) = T_n(x, z)e^{i\omega_n t} \tag{25a}$$

$$w(x, t) = W_n(x)e^{i\omega_n t} \tag{25b}$$

in which ω_n represents the nth isothermal frequency of the beam according to MSGT. Substitution of Eqs. (25a) and (25b) into Eq. (24) leads to:

$$\chi\left(i\omega_n + \frac{1}{\tau_k}\right)\nabla^2 T_n = -\omega_n^2(1 + i\omega_n\tau)\left(T_n - \frac{\Delta_E}{\alpha}z\frac{d^2 W_n}{dx^2}\right) \tag{26}$$

in which

$$\chi = \frac{k}{\rho c_v} \tag{27a}$$

$$\tau_k = \frac{k}{k^*} \tag{27b}$$

Finally, by arranging the terms of Eq. (26), the following partial differential equation (PDE) for temperature distribution in the beam is obtained:

$$\nabla^2 T_n + \beta_n^2 T_n = \beta_n^2\frac{\Delta_E}{\alpha}z\frac{d^2 W_n}{dx^2} \tag{28}$$

with

$$\beta_n^2 = \frac{\omega_n}{\chi}\frac{\tau_k\omega_n(1 + i\omega_n\tau)}{1 + i\omega_n\tau_k} \tag{29}$$

By performing mathematical calculations, the real and imaginary parts of complex parameter β_n can be separated as follows:

$$\beta_n = \sqrt{\frac{\omega_n}{\chi}}\sqrt{\varphi - i\psi} = \frac{\xi\lambda}{h} - i\frac{\xi\psi}{h\lambda} \tag{30}$$

where

$$\xi = h\sqrt{\frac{\omega_n}{2\chi}} \tag{31a}$$

$$\varphi = \frac{\tau_k\omega_n\left(1 + \tau\tau_k\omega_n^2\right)}{1 + \tau_k^2\omega_n^2} \tag{31b}$$

$$\psi = \frac{(\tau_k - \tau)\tau_k\omega_n^2}{1 + \tau_k^2\omega_n^2} \tag{31c}$$

$$\lambda = \sqrt{\varphi + \sqrt{\varphi^2 + \psi^2}} \tag{31d}$$

The general solution of partial differential equation (28) is as follows:

$$T_n(x, z) = A_n \sin(\beta_n z) + B_n \cos(\beta_n z) + \frac{\Delta_E}{\alpha} z \frac{d^2 W_n}{dx^2} \tag{32}$$

in which A_n and B_n are unknown coefficients that can be derived by imposing thermal boundary conditions. For a beam with thermally insulated upper and lower sides (i.e. $\partial T_n / \partial z = 0$ at $z = \pm h/2$), the temperature profile at different points of the beam is obtained as follows:

$$T_n(x, z) = \frac{\Delta_E}{\alpha} \left[z - \frac{\sin(\beta_n z)}{\beta_n \cos(\beta_n h/2)} \right] \frac{d^2 W_n}{dx^2} \tag{33}$$

5 Analytical solution for TED

To compute TED value in different mechanical systems, the inverse of quality factor (Q-factor) is utilized. On the basis of energy dissipation (ED) approach, the magnitude of TED is estimated by (Zener 1937):

$$Q^{-1} = \frac{1}{2\pi} \frac{\Delta U}{U_{max}} \tag{34}$$

in which ΔU and U_{max} denote the wasted thermoelastic energy and the peak value of strain energy per cycle of vibration, respectively. In a structure with volume V, the value of ΔU can be calculated via the following relation (Nowick 2012):

$$\Delta U = -\pi \iiint_V \hat{\sigma}_{ij} Im\left(\hat{\varepsilon}_{ij}^{th}\right) dV \quad \text{with} \quad \varepsilon_{ij}^{th} = \alpha\theta\delta_{ij} \tag{35}$$

In the above equation, ε_{ij}^{th} refers to the strain caused by temperature change. The symbol Im denote the imaginary part of complex variables. In addition, the hat symbol on each variable indicates the peak value of that variable in one period of vibration. With these explanations, according to Eqs. (12a), (25a) and (25b), the following relations are obtained for an Euler-Bernoulli beam:

$$\hat{\sigma}_{xx} = -Ez \frac{d^2 W_n}{dx^2} \tag{36a}$$

$$\hat{\varepsilon}_{xx}^{th} = \alpha T_n \tag{36b}$$

To derive Eq. (36a), the part related to thermal stress has been neglected owing to its small value compared to mechanical stress (Borjalilou and Asghari 2019). By placing Eqs. (36a) and (36b) into Eq. (35) and exploiting Eq. (33), one can arrive at the following relation:

$$\Delta U = \pi E \Delta_E \int_{-h/2}^{+h/2} \int_0^b \int_0^L z \left(\frac{d^2 W_n}{dx^2}\right)^2 Im\left[z - \frac{\sin(\beta_n z)}{\beta_n \cos(\beta_n h/2)}\right] dx\,dy\,dz \tag{37}$$

By performing mathematical calculations, the result of above integral is obtained as follows:

$$\Delta U = \pi E I \Delta_E Im \{[1 + F(\omega_n)]\} \int_0^L \left(\frac{d^2 W_n}{dx^2}\right)^2 dx \tag{38}$$

where $F(\omega_n)$ is a complex function with the following definition:

$$F(\omega_n) = \frac{24}{\beta_n^3 h^3} \left[\frac{\beta_n h}{2} - \tan\left(\frac{\beta_n h}{2}\right)\right] \tag{39}$$

Equation (38) can be written in a more concise form as follows:

$$\Delta U = \pi E I \Delta_E F_i \int_0^L \left(\frac{d^2 W_n}{dx^2}\right)^2 dx \tag{40}$$

Here, F_i represents the imaginary part of complex function $F(\omega_n)$. By substituting Eq. (30) into Eq. (39), one can calculate the imaginary part of $F(\omega_n)$ as follows:

$$F_i = 24\left[\frac{\psi}{\xi^2\left(\lambda^2 + \frac{\psi^2}{\lambda^2}\right)^2} - \frac{\left(3\lambda\psi - \frac{\psi^3}{\lambda^3}\right)\sin(\xi\lambda) - \left(\lambda^3 - 3\frac{\psi^2}{\lambda}\right)\sinh\left(\frac{\xi\psi}{\lambda}\right)}{\xi^3\left(\lambda^2 + \frac{\psi^2}{\lambda^2}\right)^3(\cos(\xi\lambda) + \cosh\left(\frac{\xi\psi}{\lambda}\right))}\right] \tag{41}$$

The amount of U_{max} is also computed by the following relation:

$$U_{max} = \frac{1}{2}\iiint_V (\hat{\sigma}_{ij}\hat{\varepsilon}_{ij} + \hat{p}_i\hat{\gamma}_i + \hat{\tau}_{ijk}^{(1)}\hat{\eta}_{ijk}^{(1)} + \hat{m}_{ij}^s\hat{\chi}_{ij}^s)dV \tag{42}$$

By inserting Eq. (25b) into Eqs. (9a)-(9d), one can get:

$$\hat{\varepsilon}_{xx} = -z\frac{d^2 W_n}{dx^2} \tag{43a}$$

$$\hat{\gamma}_x = -z\frac{d^3 W_n}{dx^3}, \quad \hat{\gamma}_z = -\frac{d^2 W_n}{dx^2} \tag{43b}$$

$$\hat{\eta}_{xxx}^{(1)} = -\frac{2}{5}z\frac{d^3 W_n}{dx^3}, \quad \hat{\eta}_{xyy}^{(1)} = \hat{\eta}_{yxy}^{(1)} = \hat{\eta}_{yyx}^{(1)} = \frac{1}{5}z\frac{d^3 W_n}{dx^3}$$

$$\hat{\eta}_{xxz}^{(1)} = \hat{\eta}_{xzx}^{(1)} = \hat{\eta}_{zxx}^{(1)} = -\frac{4}{15}\frac{d^2 W_n}{dx^2}, \quad \hat{\eta}_{xzz}^{(1)} = \hat{\eta}_{zxz}^{(1)} = \hat{\eta}_{zzx}^{(1)} = \frac{1}{5}z\frac{d^3 W_n}{dx^3} \tag{43c}$$

$$\hat{\eta}_{yyz}^{(1)} = \hat{\eta}_{yzy}^{(1)} = \hat{\eta}_{zyy}^{(1)} = \frac{1}{15}\frac{d^2 W_n}{dx^2}, \quad \hat{\eta}_{zzz}^{(1)} = \frac{1}{5}\frac{d^2 W_n}{dx^2}$$

$$\hat{\chi}_{xy}^s = \hat{\chi}_{yx}^s = -\frac{1}{2}\frac{d^2 W_n}{dx^2} \tag{43d}$$

Moreover, according to Eqs. (12b)-(12d), the following relations are derived for the maximum values of higher-order stresses:

$$\hat{p}_x = -2\mu l_0^2 z\frac{d^3 W_n}{dx^3}, \quad \hat{p}_z = -2\mu l_0^2\frac{d^2 W_n}{dx^2} \tag{44a}$$

$$\hat{\tau}_{xxx}^{(1)} = -\frac{4}{5}\mu l_1^2 z \frac{d^3 W_n}{dx^3}, \quad \hat{\tau}_{xyy}^{(1)} = \hat{\tau}_{yxy}^{(1)} = \hat{\tau}_{yyx}^{(1)} = \frac{2}{5}\mu l_1^2 z \frac{d^3 W_n}{dx^3}$$

$$\hat{\tau}_{xyy}^{(1)} = \hat{\tau}_{yxy}^{(1)} = \hat{\tau}_{yyx}^{(1)} = -\frac{8}{15}\mu l_1^2 \frac{d^2 W_n}{dx^2}, \quad \hat{\tau}_{xyy}^{(1)} = \hat{\tau}_{yxy}^{(1)} = \hat{\tau}_{yyx}^{(1)} = \frac{2}{5}\mu l_1^2 z \frac{d^3 W_n}{dx^3} \quad \text{(44b)}$$

$$\hat{\tau}_{xyy}^{(1)} = \hat{\tau}_{yxy}^{(1)} = \hat{\tau}_{yyx}^{(1)} = \frac{2}{15}\mu l_1^2 \frac{d^2 W_n}{dx^2}, \quad \hat{\tau}_{xyy}^{(1)} = \hat{\tau}_{yxy}^{(1)} = \hat{\tau}_{yyx}^{(1)} = \frac{2}{5}\mu l_1^2 \frac{d^2 W_n}{dx^2}$$

$$\hat{m}_{xy}^s = \hat{m}_{yx}^s = -\mu l_2^2 \frac{d^2 W_n}{dx^2} \quad \text{(44c)}$$

By putting Eqs. (36a), (43a)-(43d) and (44a)-(44c) into Eq. (42) and conducting mathematical calculations, one can achieve the relation below for U_{max}:

$$U_{max} = \frac{1}{2}\left[D_1 \int_0^L \left(\frac{d^3 W_n}{dx^3}\right)^2 dx + D_2 \int_0^L \left(\frac{d^2 W_n}{dx^2}\right)^2 dx \right] \quad \text{(45)}$$

Substitution of Eqs. (40) and (45) into Eq. (34) leads to the following relation for TED in beams with arbitrary boundary conditions according to MSGT and MGT heat conduction model:

$$Q_{MSGT}^{-1} = \frac{24 E I \Delta_E \int_0^L \left(\frac{d^2 W_n}{dx^2}\right)^2 dx}{D_1 \int_0^L \left(\frac{d^3 W_n}{dx^3}\right)^2 dx + D_2 \int_0^L \left(\frac{d^2 W_n}{dx^2}\right)^2 dx}$$

$$\times \left[\frac{\psi}{\xi^2 \left(\lambda^2 + \frac{\psi^2}{\lambda^2}\right)^2} - \frac{\left(3\lambda\psi - \frac{\psi^3}{\lambda^3}\right)\sin(\xi\lambda) - \left(\lambda^3 - 3\frac{\psi^2}{\lambda}\right)\sinh\left(\frac{\xi\psi}{\lambda}\right)}{\xi^3 \left(\lambda^2 + \frac{\psi^2}{\lambda^2}\right)^3 \left(\cos(\xi\lambda) + \cosh\left(\frac{\xi\psi}{\lambda}\right)\right)} \right] \quad \text{(46)}$$

Since in MCST, $l_0 = l_1 = 0$, one can get $D_1 = 0$ and $D_2 = EI + \mu A l_2^2$. Considering that in rectangular cross-sectional beams $A = bh$ and $I = bh^3/12$, substitution of these parameters in above equation yields the relation below for TED in the context of MCST and MGT model:

$$Q_{MCST}^{-1} = \frac{24\Delta_E}{1 + 12\frac{\mu}{E}\left(\frac{l_2}{h}\right)^2}$$

$$\times \left[\frac{\psi}{\xi^2 \left(\lambda^2 + \frac{\psi^2}{\lambda^2}\right)^2} - \frac{\left(3\lambda\psi - \frac{\psi^3}{\lambda^3}\right)\sin(\xi\lambda) - \left(\lambda^3 - 3\frac{\psi^2}{\lambda}\right)\sinh\left(\frac{\xi\psi}{\lambda}\right)}{\xi^3 \left(\lambda^2 + \frac{\psi^2}{\lambda^2}\right)^3 \left(\cos(\xi\lambda) + \cosh\left(\frac{\xi\psi}{\lambda}\right)\right)} \right] \quad \text{(47)}$$

The above relationship is exactly the same as the one derived by Singh et al. (2022) on the basis of CF approach. For a beam with simply-supported (SS) boundary conditions, one can write:

$$W_n(x) = \sin(\Lambda_n x) \quad \text{with} \quad \Lambda_n = \frac{n\pi}{L} \quad \text{(48)}$$

It can be clearly seen that the above shape function exactly satisfies both the isothermal form of the motion equation (15) and the isothermal form of the boundary conditions presented in Eqs. (16a)-(16c). By inserting Eq. (48) into Eq. (46) and computing the integrals

in it, one can attain the following relation for TED in SS beams:

$$Q^{-1} = \frac{24EI\Delta_E}{\Lambda_n^2 D_1 + D_2}$$

$$\times \left[\frac{\psi}{\xi^2 \left(\lambda^2 + \frac{\psi^2}{\lambda^2}\right)^2} - \frac{\left(3\lambda\psi - \frac{\psi^3}{\lambda^3}\right)\sin(\xi\lambda) - \left(\lambda^3 - 3\frac{\psi^2}{\lambda}\right)\sinh\left(\frac{\xi\psi}{\lambda}\right)}{\xi^3 \left(\lambda^2 + \frac{\psi^2}{\lambda^2}\right)^3 \left(\cos(\xi\lambda) + \cosh\left(\frac{\xi\psi}{\lambda}\right)\right)} \right] \quad (49)$$

Note that in this type of boundary conditions, to calculate size-dependent ω_n, it is enough to insert Eqs. (25b) and (48) into Eq. (15) to reach the following relationship:

$$\omega_n = \Lambda_n^2 \sqrt{\frac{\Lambda_n^2 D_1 + D_2}{\rho A}} \quad (50)$$

6 Results and discussion

To evaluate the correctness of the developed model, a comparison study is firstly carried out. For this aim, the results extracted by the presented formulation are compared with those reported by Zhang and Li (2020) in a certain case. By employing the complex frequency (CF) approach, Zhang and Li (2020) established an analytical framework for calculating TED value in functionally graded (FG) microbeams according to MCST and the Fourier model. Hence, to compare the results of this research with those of Zhang and Li (2020), length scale parameters l_0 and l_1 as well as material constants τ and k^* must be ignored in the obtained TED relation. Also, the microbeam material should be considered homogeneous and full ceramic. In this case, the material of microbeam will be alumina (Al_2O_3), whose characteristics at the reference temperature $T_0 = 300$ K are: $E = 380$ GPa, $\rho = 3800$ kg/m^3, $c_v = 750$ J/kgK, $\alpha = 7.4 * 10^{-6}$ 1/ K, $k = 10$ W/mK and $\nu = 0.23$. Based on the formulation proposed in this work and that derived by Zhang and Li (2020), the variations of TED with the thickness of a SS beam with the length $L = 500$ μm at the first vibration mode are depicted in Fig. 2. In this figure, the length scale parameter is assumed to be $l_2 = 15$ μm. It can be readily seen that the curve extracted based on the presented model is consistent with the one presented by Zhang and Li (2020).

In the following, with the aid of the solution established in the current research, several numerical examples are provided to perform an embracing parametric analysis on the influence of some determining factors like characteristic lengths of MSGT, nonclassical parameters of MGT model, beam thickness, aspect ratio of the beam, vibration mode number and material on the amount and pattern of TED. With the exception of the cases that will be explained, in other cases, numerical results are given for a SS beam made of silicon with an aspect ratio of $L/h = 20$. The mechanical and thermal properties of silicon (Si) as well as gold (Au) and copper (Cu) at $T_0 = 300$ K can be seen in Table 1 (Singh et al. 2022; Fredi et al. 2020). The point to be noted here is that to extract the results in the framework of MCST, $l_0 = l_1 = 0$ and $l_2 = l$ are placed in the presented relations. Moreover, it is customary that to derive the results corresponding to MSGT, all three material length scale parameters are considered equal to $l_0 = l_1 = l_2 = l$ (Lam et al. 2003).

The changes of TED with beam thickness within the framework of CT, MCST and MSGT are displayed in Fig. 3 by assuming $l = 0.5$ μm. Figures 3a and 3b are drawn for the cases $n = 1$ and $n = 10$, respectively. As it is clear, among the three investigated theories, CT and

Fig. 2 Validation analysis by comparing the variations of TED with those reported in the literature
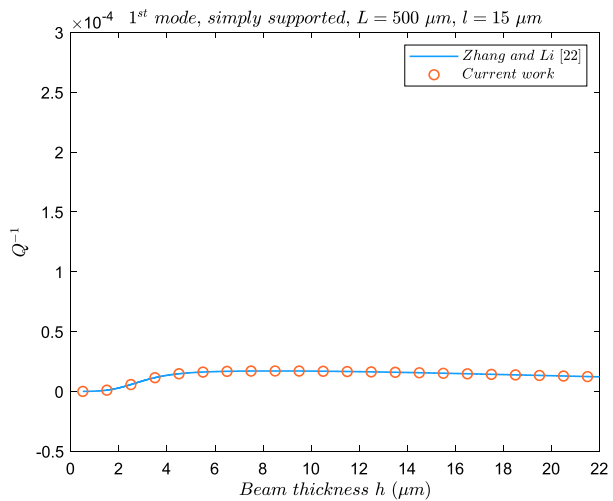

**Table 1** Properties of silicon (Si), gold (Au) and copper (Cu) at $T_0 = 300$ K

Property	Si	Au	Cu
E (GPa)	169	79	110
ρ (kg/m³)	2330	19300	8940
c_v (J/kgK)	713	129.1	385.9
α (10^{-6}/K)	2.6	14.2	16.5
k (W/mK)	70	315	386
k^* (W/mKs)	157	150	70
τ (ps)	3.95	93.5	27.3

MSGT predict the highest and lowest amounts for TED, respectively. The thickness at which the peak value of TED comes about is called critical thickness. According to the curves of Fig. 3, the critical thickness estimated by MSGT is higher than that computed by MCST and CT. Another important matter that can be pointed out in Figs. 3a and 3b is that as the beam thickness gets larger, the estimations of MCST and MSGT approach those of CT. This well authenticates the diminution of small-scale effect in larger dimensions. The comparison of Figs. 3a and 3b reveals that although in the case of $n = 10$, the predicted value for TED by CT, MCST and MSGT is lower than in the case of $n = 1$, but the difference between the results of these three theories is greater.

Figure 4 illustrates TED versus beam thickness for four different values of the length scale parameter in the framework of MSGT. Figures 4a and 4b are plotted for the cases $n = 1$ and $n = 10$, respectively. By looking at the graphs in this figure, it can be easily found that by increasing the amount of l, TED value tapers off and the amount of critical thickness ascends. It is also evident in this figure that with the increase of beam thickness, the effect of size gradually lessens and the obtained results converge to the prediction of CT. It can also be observed that in the case of $n = 10$, both TED value and critical thickness are calculated lower than in the case of $n = 1$.

In Fig. 5, TED diagrams as a function of beam thickness are drawn according to the Fourier and MGT models. Based on the relations of MSGT, $l = 2$ μm is assumed to derive these graphs. Also, in Figs. 5a and 5b, the vibration mode number n is assumed equal to 1

Fig. 3 TED versus beam thickness according to CT, MCST and MSGT for the case $l = 0.5\ \mu m$ (a) $n = 1$ (b) $n = 10$
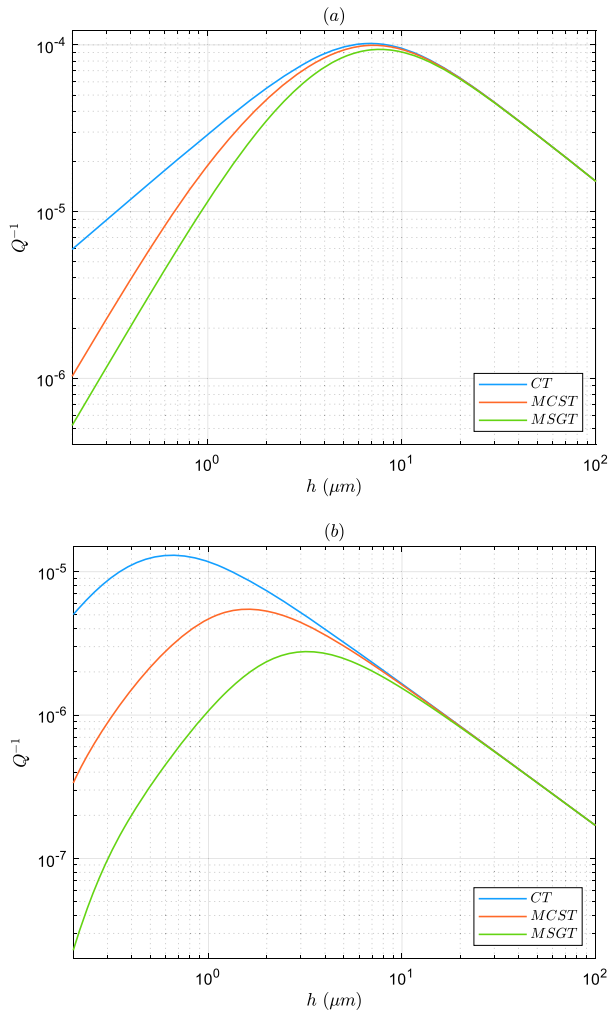
and 10, respectively. As it is obvious, in the case of $n = 1$, the difference between the estimations of Fourier and MGT models is trifling, and only in very small thicknesses, compared to the Fourier model, MGT model anticipates a higher amount for TED with a small difference. According to Fig. 5b, with the increase of the vibration mode from 1 to 10, the difference between the results of Fourier and MGT models intensifies. Besides, in this vibration mode, TED value obtained by the Fourier model is higher than that computed by MGT model. In this way, it can be concluded that the impact of utilizing MGT model is more specific in higher vibration modes. It should be noted that despite the difference between the results of Fourier and MGT models in the vibration mode number $n = 10$, in this case as the beam thickness enlarges, this difference becomes smaller and smaller, which is a sign of reduction of size effect on thermal domain.

TED variations versus vibration mode number n according to CT, MCST and MSGT are depicted in Fig. 6. To draw these graphs, $h = 1\ \mu m$ and $l = 0.5\ \mu m$ are considered. As can be observed, for all examined vibration modes, CT estimates the highest and MSGT

Fig. 4 Effect of length scale
parameter on TED variations
with beam thickness in the
framework of MSGT (a) $n = 1$
(b) $n = 10$
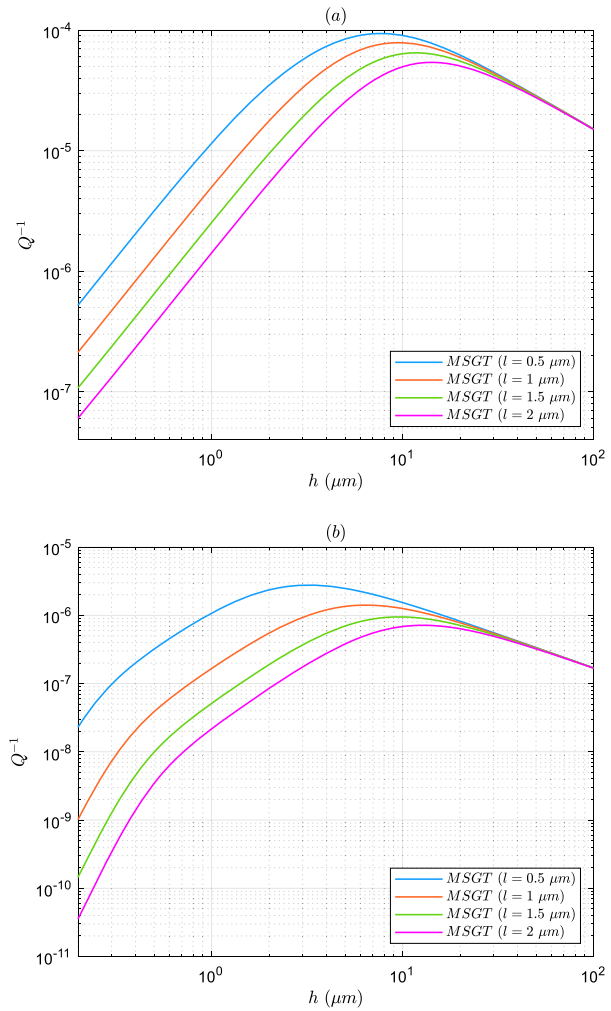
the lowest values for TED. It is also clear that the maximum TED value for CT occurs in the third vibration mode and for MCST and MSGT in the second vibration mode, and then with the increase in the vibration mode number, TED diagram follows a downward trend. This result can be explained by the fact that the temperature field in the beam arrives at equilibrium in a certain time indicated by τ^*. At low vibration modes that correspond to low frequencies, one can write $\tau^* \ll \omega_n^{-1}$. Hence, because the vibration period is long, the microbeam is in isothermal situation and remains in equilibrium condition. In this way, the magnitude of wasted energy is small. At high vibration modes that correspond to high frequencies (that is $\tau^* \gg \omega_n^{-1}$), the microbeam hasn't sufficient time to relax. So, similar to that explained for the situation $\tau^* \ll \omega_n^{-1}$, a slight amount of energy dissipation occurs. Accordingly, the maximum amount of TED happens at $\tau^* \approx \omega_n^{-1}$, which corresponds to intermediate vibration modes.

According to the relation obtained by MSGT, for four different values of length scale parameter (i.e. $l = 0.5, 1, 1.5$ and 2 μm), Fig. 7 displays the alterations of TED with vibration mode number. The curves of this figure are plotted for a beam with thickness $h = 1$ μm. By

Fig. 5 TED versus beam thickness on the basis of Fourier and MGT models for the case $l = 2$ μm (a) $n = 1$ (b) $n = 10$
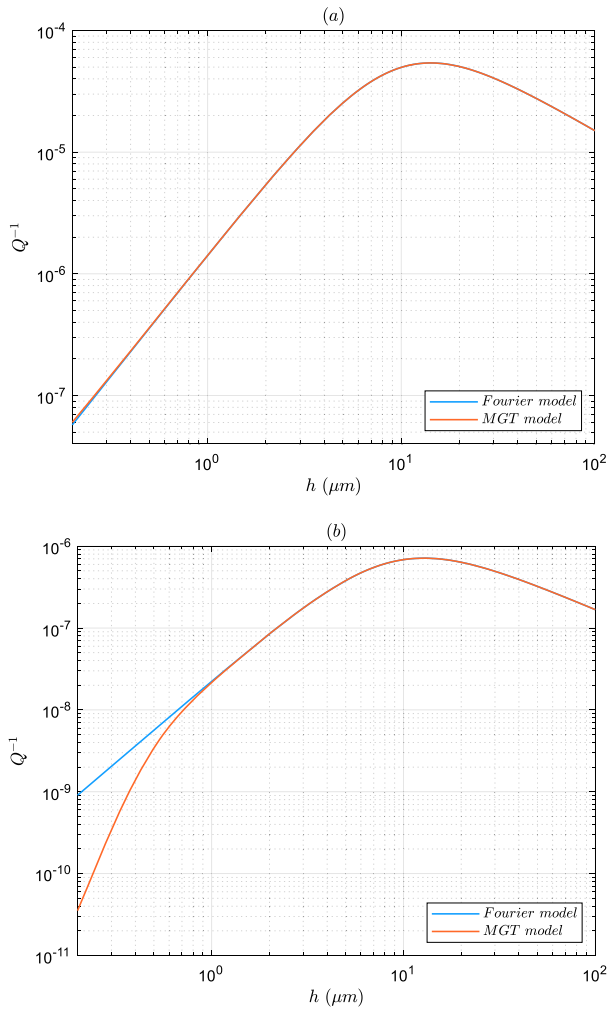
observing these curves, it can be inferred that when the length scale parameter enlarges, the amount of TED diminishes for all vibration modes. In addition, except for case $l = 0.5$ μm, where the peak value of TED takes place at $n = 2$, in the rest of the cases, the peak value of TED happens at $n = 1$, and the graph of TED in terms of vibration mode number n is completely descending.

On the basis of MSGT, the influence of the Fourier and MGT models on TED variations with vibration mode number is assessed in Fig. 8. To extract these results, $l = 2$ μm and $h = 1$ μm are adopted. According to these diagrams, it can be said that the Fourier and MGT models have almost the same prediction for the value of TED in low vibration modes (that is $n < 10$), but with the increase of vibration mode number, the difference between the outcomes of these two models is augmented. As it is apparent, in higher vibration modes, MGT model estimates a lower value for TED than the Fourier model. The physical justification of this outcome can be that the propagation velocity of heat based on the Fourier law is infinite, whereas the velocity predicted by MGT model is finite. Therefore, the heat induced in the

Fig. 6 TED versus vibration mode number according to CT, MCST and MSGT for the case $h = 1$ μm and $l = 0.5$ μm

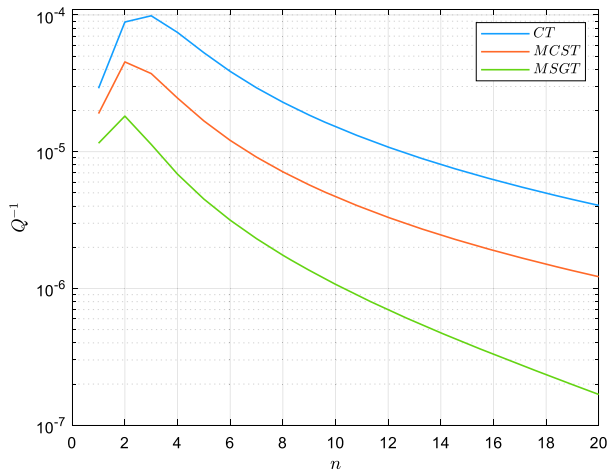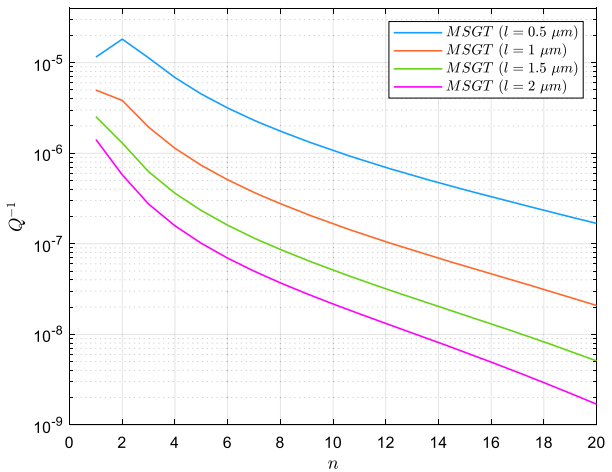**Fig. 7** Effect of length scale parameter on TED variations with vibration mode number in the framework of MSGT for the case $h = 1$ μm

framework of MGT model has less time to propagate during a cycle of oscillation, which yields smaller amount of thermal energy dissipation. Consequently, the amount of TED corresponding to MGT model is less than that estimated by the Fourier model. It is also easy to see that according to the predictions of both Fourier and MGT models, when the vibration mode takes larger values, the amount of TED abates.

In the framework of CT, MCST and MSGT, the alterations of TED versus aspect ratio L/h are demonstrated in Fig. 9. To plot these curves, $h = 1$ μm and $l = 0.5$ μm are assumed. In addition, the diagrams are drawn for vibration mode number $n = 10$. In this figure, it is clear that among the three evaluated theories, TED value approximated by MSGT has the lowest amount compared to the other two theories. This result originates from the fact that by accounting for nonclassical kinematic parameters and their conjugate stresses in MCST and MSGT, the value of elastic energy of the beam gets greater and accordingly, the ratio of dissipated thermal energy to stored energy in the resonator diminishes. In addition, the elastic energy calculated in the framework of MSGT is higher than that obtained based on MCST. Therefore, in general, it is quite expected that MSGT predicts the highest and CT

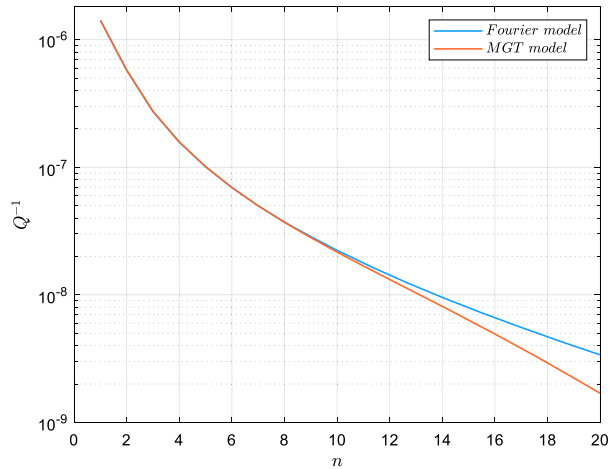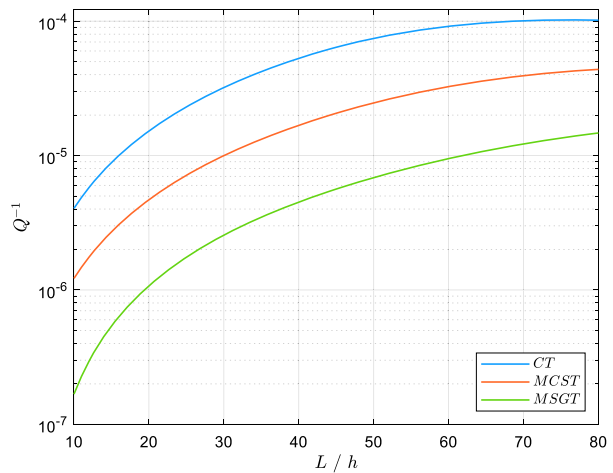**Fig. 8** TED versus vibration mode number based on Fourier and MGT models for the case $h = 1$ μm

Fig. 9 TED versus aspect ratio according to CT, MCST and MSGT for the case $h = 1$ μm, $l = 0.5$ μm and $n = 10$

the lowest value for TED. It can also be seen that according to the prediction of all three used theories, with the increase of the aspect ratio of beam, TED is generally strengthened.

Within the framework of MSGT, for four different amounts of material length scale parameter l, Fig. 10 indicates TED diagram as a function of aspect ratio. These curves are drawn for a beam with thickness $h = 1$ μm at vibration mode number $n = 10$. According to the curves of this figure, in the entire range considered for aspect ratio L/h, for larger values of l, a smaller amount for TED is estimated. In addition, with the increase of the value of L/h, TED value heightens for all four values considered for l.

By employing the relation of TED provided by MSGT, the effect of the Fourier and MGT models on TED alterations with aspect ratio is analyzed in Fig. 11. To draw this figure, $l = 2$ μm and $h = 1$ μm are assumed. In addition, the vibration mode number is considered to be $n = 10$. This figure reveals that for small aspect ratios, the MGT model predicts lower values for TED compared to the Fourier model, as the aspect ratio and the beam size ascend, the small-scale effect on thermal field dwindles and the estimations of MGT model approach those of the Fourier model.

Fig. 10 Effect of length scale parameter on TED variations with aspect ratio in the framework of MSGT for the case $h = 1$ μm and $n = 10$
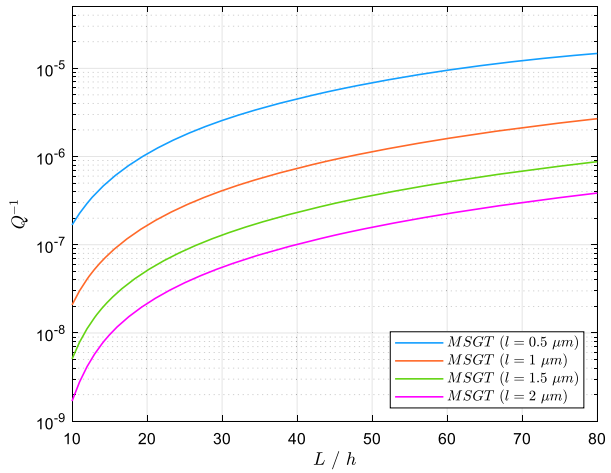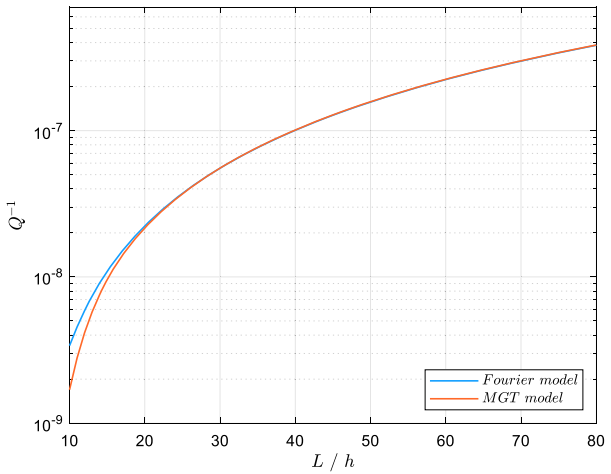

Fig. 11 TED versus aspect ratio based on Fourier and MGT models for the case $h = 1$ μm and $n = 10$


To appraise the influence of the type of material on TED value, the graphs of changes of TED with the dimensionless parameter h/l for three materials silicon (Si), gold (Au) and copper (Cu) are depicted in Fig. 12. These curves are drawn for a beam with thickness $h = 1$ μm at vibration mode number $n = 1$. As can be seen, for all three studied materials, the estimation of MSGT for TED is lower than that of MCST. Another point is that by increasing the value of h/l, which is equivalent to reducing the size effect, the difference between the outputs of MCST and MSGT shrinks and the predictions of both theories converge to the value calculated by CT. Also, according to these curves, the highest amount of TED occurs in the beam made of copper and the lowest in the gold beam. The results of this figure can be momentous because by choosing the suitable material, TED value can be reduced.

7 Conclusions

In the current investigation, by accommodating the impact of size into both constitutive relations and heat equation through the modified strain gradient theory (MSGT) and Moore-

Fig. 12 Influence of material on TED in the framework of MCST and MSGT for the case $h = 1$ μm and $n = 1$
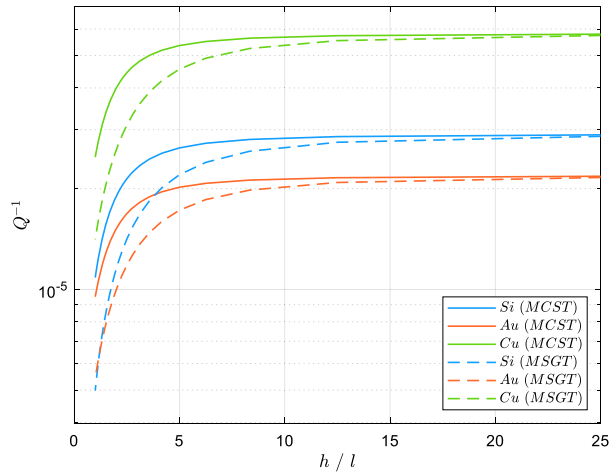
Gibson-Thompson (MGT) heat conduction model, a new nonclassical framework has been provided to estimate scale-dependent value of thermoelastic damping (TED) in microbeam resonators. Initially, the constitutive relations and heat equation have been established on the basis of MSGT and MGT model. After solving the MGT-based heat equation and arriving at the temperature field, the maximum amounts of elastic and wasted thermal energies in one period of beam oscillation have been calculated. Then, by applying the TED relation in the context of energy dissipation (ED) approach, a closed-form solution involving the specific parameters of MSGT and MGT model has been presented for TED. By comparing the results extracted via the developed model with those available in the literature, a comparison between different described models and obtained results has been carried out. To address the relation between TED value and some factors like characteristic parameters of MSGT and MGT model, geometrical parameters including the thickness and aspect ratio of the beam, vibration mode number and material, various numerical data have been prepared. Based on the obtained results, the significant outcomes of the paper at hand can be expressed concisely as follows:

- The incorporation of the length scale parameter into the governing equations leads to a diminution in the amount of TED compared to the classical theory (CT).
- TED value computed by the modified strain gradient theory (MSGT) is lower than that determined by the modified couple stress theory (MCST).
- The greater amounts of the length scale parameters of MSGT, the smaller TED value predicted by this theory.
- At bigger scales and lower vibration modes, the difference between the estimations of the Fourier and MGT models is meager, but at smaller dimensions and higher vibration modes, TED value specified by MGT model is less than that extracted by the Fourier model.
- By and large, without regard to the kind of continuum mechanics theory or heat conduction model, by getting larger the vibration mode number in the range of $1 \leq n \leq 20$, TED value lessens.
- Based on the prediction of MSGT and MGT model, among the examined materials (i.e. silicon, gold and copper), the highest TED value belongs to the copper beam and the lowest one occurs in the gold beam.

- As the value of dimensionless ratio h/l heightens, irrespective of the material of the beam, the difference between TED values obtained by MCST and MSGT declines and the predictions of these two theories approach the amount computed by CT.

Data Availability The data that support the findings of this study are available on request from the corresponding author.

Declarations

Competing interests The authors declare no competing interests.

References

Abbas, I.A.: A two-temperature model for evaluation of thermoelastic damping in the vibration of a nanoscale resonators. Mech. Time-Depend. Mater. **20**, 511–522 (2016)

Abedi, M., Tan, X., Klausner, J.F., Bénard, A.: Solar desalination chimneys: investigation on the feasibility of integrating solar chimneys with humidification–dehumidification systems. Renew. Energy **202**, 88–102 (2023). https://doi.org/10.1016/j.renene.2022.11.069

Abouelregal, A.E., Mohammad-Sedighi, H., Faghidian, S.A., Shirazi, A.H.: Temperature-dependent physical characteristics of the rotating nonlocal nanobeams subject to a varying heat source and a dynamic load. Facta Univ., Mech. Eng. **19**(4), 633–656 (2021)

Akbarzadeh Khorshidi, M.: Postbuckling of viscoelastic micro/nanobeams embedded in visco-Pasternak foundations based on the modified couple stress theory. Mech. Time-Depend. Mater. **25**(2), 265–278 (2021)

Akgöz, B., Civalek, Ö.: Longitudinal vibration analysis for microbars based on strain gradient elasticity theory. J. Vib. Control **20**(4), 606–616 (2014)

Ansari, R., Gholami, R., Sahmani, S.: Size-dependent vibration of functionally graded curved microbeams based on the modified strain gradient elasticity theory. Arch. Appl. Mech. **83**, 1439–1449 (2013)

Atta, D., Abouelregal, A.E., Sedighi, H.M., Alharb, R.A.: Thermodiffusion interactions in a homogeneous spherical shell based on the modified Moore–Gibson–Thompson theory with two time delays. Mech. Time-Depend. Mater., 1–22 (2023)

Borjalilou, V., Asghari, M.: Small-scale analysis of plates with thermoelastic damping based on the modified couple stress theory and the dual-phase-lag heat conduction model. Acta Mech. **229**, 3869–3884 (2018)

Borjalilou, V., Asghari, M.: Size-dependent strain gradient-based thermoelastic damping in micro-beams utilizing a generalized thermoelasticity theory. Int. J. Appl. Mech. **11**(1), 1950007 (2019)

Borjalilou, V., Asghari, M., Bagheri, E.: Small-scale thermoelastic damping in micro-beams utilizing the modified couple stress theory and the dual-phase-lag heat conduction model. J. Therm. Stresses **42**(7), 801–814 (2019)

Borjalilou, V., Asghari, M., Taati, E.: Thermoelastic damping in nonlocal nanobeams considering dual-phase-lagging effect. J. Vib. Control **26**(11–12), 1042–1053 (2020)

Dastjerdi, S., Abbasi, M.: A new approach for time-dependent response of viscoelastic graphene sheets embedded in visco-Pasternak foundation based on nonlocal FSDT and MHSDT theories. Mech. Time-Depend. Mater. **24**, 329–361 (2020)

Delfani, M.R., Taaghi, S., Tavakol, E.: Uniform motion of an edge dislocation within Mindlin's first strain gradient elasticity. Int. J. Mech. Sci. **179**, 105701 (2020)

Ebrahimi-Mamaghani, A., Mirtalebi, S.H., Ahmadian, M.T.: Magneto-mechanical stability of axially functionally graded supported nanotubes. Mater. Res. Express **6**(12), 1250c5 (2020)

Emami, A.A., Alibeigloo, A.: Exact solution for thermal damping of functionally graded Timoshenko microbeams. J. Therm. Stresses **39**(2), 231–243 (2016)

Eringen, A.C.: On differential equations of nonlocal elasticity and solutions of screw dislocation and surface waves. J. Appl. Phys. **54**(9), 4703–4710 (1983)

Esfahani, S., Esmaeilzade Khadem, S., Ebrahimi Mamaghani, A.: Size-dependent nonlinear vibration of an electrostatic nanobeam actuator considering surface effects and inter-molecular interactions. Int. J. Mech. Mater. Des. **15**, 489–505 (2019)

Fang, J., Näsholm, S.P., Chen, W., Holm, S.: The fractional constitutive models for nonlocal material based on scattering wave equations. Mech. Time-Depend. Mater., 1–23 (2020)

Fredi, G., Dorigato, A., Pegoretti, A.: Dynamic-mechanical response of carbon fiber laminates with a reactive thermoplastic resin containing phase change microcapsules. Mech. Time-Depend. Mater. **24**(3), 395–418 (2020)

Ge, Y., Sarkar, A.: Thermoelastic damping in vibrations of small-scaled rings with rectangular cross-section by considering size effect on both structural and thermal domains. Int. J. Struct. Stab. Dyn. **23**, 2350026 (2022)

Ghayesh, M.H., Amabili, M., Farokhi, H.: Nonlinear forced vibrations of a microbeam based on the strain gradient elasticity theory. Int. J. Eng. Sci. **63**, 52–60 (2013)

Green, A.E., Naghdi, P.: Thermoelasticity without energy dissipation. J. Elast. **31**(3), 189–208 (1993)

Grover, D., Seth, R.K.: Generalized viscothermoelasticity theory of dual-phase-lagging model for damping analysis in circular micro-plate resonators. Mech. Time-Depend. Mater. **23**, 119–132 (2019)

Gu, B., He, T., Ma, Y.: Thermoelastic damping analysis in micro-beam resonators considering nonlocal strain gradient based on dual-phase-lag model. Int. J. Heat Mass Transf. **180**, 121771 (2021)

Guyer, R.A., Krumhansl, J.A.: Solution of the linearized phonon Boltzmann equation. Phys. Rev. **148**(2), 766 (1966)

Hassena, M.A.B., Samaali, H., Ouakad, H.M., Najar, F.: 2D electrostatic energy harvesting device using a single shallow arched microbeam. Int. J. Non-Linear Mech. **132**, 103700 (2021)

Jalil, A.T., AbdulAmeer, S.A., Hassan, Y.M., Mohammed, I.M., Ali, M.J., Ward, Z.H., Ghasemi, S.: Analytical model for thermoelastic dissipation in oscillations of toroidal micro/nanorings in the context of Guyer-Krumhansl heat equation. Int. J. Struct. Stab. Dyn. (2023)

Jalil, A.T., Karim, N., Ruhaima, A.A.K., Sulaiman, J.M.A., Hameed, A.S., Abed, A.S., et al., Rayani, Y.: Analytical model for thermoelastic damping in in-plane vibrations of circular cross-sectional micro/nanorings with dual-phase-lag heat conduction. J. Vibr. Eng. Technol., 1–14 (2023)

Jalil, A.T., Saleh, Z.M., Imran, A.F., Yasin, Y., Ruhaima, A.A.K., Gatea, M.A., Esmaeili, S.: A size-dependent generalized thermoelasticity theory for thermoelastic damping in vibrations of nanobeam resonators. Int. J. Struct. Stab. Dyn. **23**, 2350133 (2023)

Kim, J.H., Kim, J.H.: Dual-phase-lagging thermoelastic dissipation for toroidal micro/nano-ring resonator model. Therm. Sci. Eng. Prog. **39**, 101683 (2023)

Kumar, R.: Effect of phase-lag on thermoelastic vibration of Timoshenko beam. J. Therm. Stresses **43**(11), 1337–1354 (2020)

Kumar, R.: Analysis of the quality factor of micromechanical resonators using memory-dependent derivative under different models. Arch. Appl. Mech. **91**(6), 2735–2745 (2021)

Kumar, R., Kumar, R.: Effect of two-temperature parameter on thermoelastic vibration in micro and nano beam resonator. Eur. J. Mech. A, Solids **89**, 104310 (2021)

Kumar, H., Mukhopadhyay, S.: Thermoelastic damping analysis in microbeam resonators based on Moore–Gibson–Thompson generalized thermoelasticity theory. Acta Mech. **231**(7), 3003–3015 (2020)

Kumar, R., Kumar, R., Kumar, H.: Effects of phase-lag on thermoelastic damping in micromechanical resonators. J. Therm. Stresses **41**(9), 1115–1124 (2018)

Kumar, R., Tiwari, R., Kumar, R.: Significance of memory-dependent derivative approach for the analysis of thermoelastic damping in micromechanical resonators. Mech. Time-Depend. Mater. **26**(1), 101–118 (2022)

Lam, D.C., Yang, F., Chong, A.C.M., Wang, J., Tong, P.: Experiments and theory in strain gradient elasticity. J. Mech. Phys. Solids **51**(8), 1477–1508 (2003)

Li, F., Esmaeili, S.: On thermoelastic damping in axisymmetric vibrations of circular nanoplates: incorporation of size effect into structural and thermal areas. Eur. Phys. J. Plus **136**(2), 1–17 (2021)

Li, M., Cai, Y., Bao, L., Fan, R., Zhang, H., Wang, H., Borjalilou, V.: Analytical and parametric analysis of thermoelastic damping in circular cylindrical nanoshells by capturing small-scale effect on both structure and heat conduction. Arch. Civ. Mech. Eng. **22**, 1–16 (2022)

Li, M., Cai, Y., Fan, R., Wang, H., Borjalilou, V.: Generalized thermoelasticity model for thermoelastic damping in asymmetric vibrations of nonlocal tubular shells. Thin-Walled Struct. **174**, 109142 (2022)

Lifshitz, R., Roukes, M.L.: Thermoelastic damping in micro-and nanomechanical systems. Phys. Rev. B **61**(8), 5600 (2000)

Lim, C.W., Zhang, G., Reddy, J.: A higher-order nonlocal elasticity and strain gradient theory and its applications in wave propagation. J. Mech. Phys. Solids **78**, 298–313 (2015)

Liu, D., Geng, T., Wang, H., Esmaeili, S.: Analytical solution for thermoelastic oscillations of nonlocal strain gradient nanobeams with dual-phase-lag heat conduction. Mech. Based Des. Struct. Mach., 1–31 (2021)

Loghman, A., Moradi, M.: The analysis of time-dependent creep in FGPM thick walled sphere under electro-magneto-thermo-mechanical loadings. Mech. Time-Depend. Mater. **17**, 315–329 (2013)

Lord, H.W., Shulman, Y.: A generalized dynamical theory of thermoelasticity. J. Mech. Phys. Solids **15**(5), 299–309 (1967)

Luo, C., Wang, L., Xie, Y., Chen, B.: A new conjugate gradient method for moving force identification of vehicle–bridge system. J. Vibr. Eng. Technol., 1–18 (2022). https://doi.org/10.1007/s42417-022-00824-1

Malikan, M.: Analytical predictions for the buckling of a nanoplate subjected to non-uniform compression based on the four-variable plate theory. J. Appl. Comput. Mech. **3**, 218–228 (2017)

Malikan, M., Eremeyev, V.A.: On time-dependent nonlinear dynamic response of micro-elastic solids. Int. J. Eng. Sci. **182**, 103793 (2023). https://doi.org/10.1016/j.ijengsci.2022.103793

Malikan, M., Eremeyev, V.A.: On dynamic modeling of piezomagnetic/flexomagnetic microstructures based on Lord–Shulman thermoelastic model. Arch. Appl. Mech. **93**(1), 181–196 (2023)

Malikan, M., Nguyen, V.B.: Buckling analysis of piezo-magnetoelectric nanoplates in hygrothermal environment based on a novel one variable plate theory combining with higher-order nonlocal strain gradient theory. Physica E, Low-Dimens. Syst. Nanostruct. **102**, 8–28 (2018)

Malikan, M., Dimitri, R., Tornabene, F.: Effect of sinusoidal corrugated geometries on the vibrational response of viscoelastic nanoplates. Appl. Sci. **8**(9), 1432 (2018)

Malikan, M., Eremeyev, V.A., Sedighi, H.M.: Buckling analysis of a non-concentric double-walled carbon nanotube. Acta Mech. **231**(12), 5007–5020 (2020b)

Malikan, M., Eremeyev, V.A., Żur, K.K.: Effect of axial porosities on flexomagnetic response of in-plane compressed piezomagnetic nanobeams. Symmetry **12**(12), 1935 (2020a)

Malikan, M., Krasheninnikov, M., Eremeyev, V.A.: Torsional stability capacity of a nano-composite shell based on a nonlocal strain gradient shell model under a three-dimensional magnetic field. Int. J. Eng. Sci. **148**, 103210 (2020)

Mindlin, R.D., Eshel, N.: On first strain-gradient theories in linear elasticity. Int. J. Solids Struct. **4**(1), 109–124 (1968)

Mindlin, R.D., Tiersten, H.: Effects of Couple-Stresses in Linear Elasticity. Columbia University Press, New York (1962)

Mirfatah, S.M., Shahmohammadi, M.A., Salehipour, H., Civalek, Ö.: Size-dependent dynamic stability of nanocomposite enriched micro-shell panels in thermal environment using the modified couple stress theory. Eng. Anal. Bound. Elem. **143**, 483–500 (2022)

Mousavi, S.M., Paavola, J.: Analysis of plate in second strain gradient elasticity. Arch. Appl. Mech. **84**, 1135–1143 (2014)

Nowick, A.S.: Anelastic Relaxation in Crystalline Solids (Vol. 1). Elsevier, Amsterdam (2012)

Panahi, R., Asghari, M., Borjalilou, V.: Nonlinear forced vibration analysis of micro-rotating shaft–disk systems through a formulation based on the nonlocal strain gradient theory. Arch. Civ. Mech. Eng. **23**(2), 1–32 (2023)

Peng, Y., Sun, Y., Luo, G., Wu, G., Zhang, T.: Recent advancements in inertial micro-switches. Electronics **8**(6), 648 (2019)

Peng, W., Tian, L., He, T.: Dual-phase-lag thermoviscoelastic analysis of a size-dependent microplate based on a fractional-order heat-conduction and strain model. Mech. Time-Depend. Mater., 1–22 (2022)

Potapov, V.D.: About the stability of nonlocal viscoelastic struts lying on an elastic foundation. Mech. Time-Depend. Mater. **19**, 35–42 (2015)

Prabhakar, S., Vengallatore, S.: Theory of thermoelastic damping in micromechanical resonators with two-dimensional heat conduction. J. Microelectromech. Syst. **17**(2), 494–502 (2008)

Quintanilla, R.: Moore–Gibson–Thompson thermoelasticity. Math. Mech. Solids **24**(12), 4020–4031 (2019)

Rezazadeh, G., Vahdat, A.S., Tayefeh-rezaei, S., Cetinkaya, C.: Thermoelastic damping in a micro-beam resonator using modified couple stress theory. Acta Mech. **223**, 1137–1152 (2012)

Sarparast, H., Alibeigloo, A., Borjalilou, V., Koochakianfard, O.: Forced and free vibrational analysis of viscoelastic nanotubes conveying fluid subjected to moving load in hygro-thermo-magnetic environments with surface effects. Arch. Civ. Mech. Eng. **22**(4), 172 (2022)

Shi, X., Qing, W., Marhaba, T., Zhang, W.: Atomic force microscopy-scanning electrochemical microscopy (AFM-SECM) for nanoscale topographical and electrochemical characterization: principles, applications and perspectives. Electrochim. Acta **332**, 135472 (2020)

Shi, T., Liu, Y., Hu, Z., Cen, M., Zeng, C., Xu, J., Zhao, Z.: Deformation performance and fracture toughness of carbon nanofiber-modified cement-based materials. ACI Mater. J. **119**(5), 119–128 (2022). https://doi.org/10.14359/51735976

Singh, B., Kumar, H., Mukhopadhyay, S.: Thermoelastic damping analysis in micro-beam resonators in the frame of modified couple stress and Moore–Gibson–Thompson (MGT) thermoelasticity theories. Waves Random Complex Media, 1–18 (2021)

Singh, B., Kumar, H., Mukhopadhyay, S.: Analysis of size effects on thermoelastic damping in the Kirchhoff's plate resonator under Moore–Gibson–Thompson thermoelasticity. Thin-Walled Struct. **180**, 109793 (2022)

Sun, X., Chen, Z., Guo, K., Fei, J., Dong, Z., Xiong, H.: Geopolymeric flocculation-solidification of tail slurry of shield tunnelling spoil after sand separation. Constr. Build. Mater. **374**, 130954 (2023). https://doi.org/10.1016/j.conbuildmat.2023.130954

Sun, X., Chen, Z., Sun, Z., Wu, S., Guo, K., Dong, Z., Peng, Y.: High-efficiency utilization of waste shield slurry: a geopolymeric flocculation-filtration-solidification method. Constr. Build. Mater. **387**, 131569 (2023). https://doi.org/10.1016/j.conbuildmat.2023.131569

Tadi Beni, Z., Hosseini Ravandi, S.A., Tadi Beni, Y.: Size-dependent nonlinear forced vibration analysis of viscoelastic/piezoelectric nano-beam. J. Appl. Comput. Mech. (2020)

Tiwari, R., Abouelregal, A.E., Shivay, O.N., Megahid, S.F.: Thermoelastic vibrations in electro-mechanical resonators based on rotating microbeams exposed to laser heat under generalized thermoelasticity with three relaxation times. Mech. Time-Depend. Mater., 1–25 (2022)

Tunvir, K., Ru, C.Q., Mioduchowski, A.: Large-deflection effect on thermoelastic dissipation of microbeam resonators. J. Therm. Stresses **35**(12), 1076–1094 (2012)

Tzou, D.Y.: A unified field approach for heat conduction from macro-to micro-scales (1995)

Tzou, D.Y., Guo, Z.Y.: Nonlocal behavior in thermal lagging. Int. J. Therm. Sci. **49**(7), 1133–1137 (2010)

Uzun, B., Civalek, Ö., Yaylı, M.Ö.: Torsional and axial vibration of restrained saturated nanorods via strain gradient elasticity. Arch. Appl. Mech. **93**(4), 1605–1630 (2023)

Xiao, C., Zhang, G., Hu, P., Yu, Y., Mo, Y., Borjalilou, V.: Size-dependent generalized thermoelasticity model for thermoelastic damping in circular nanoplates. Waves Random Complex Media, 1–21 (2021)

Yang, F.A.C.M., Chong, A.C.M., Lam, D.C.C., Tong, P.: Couple stress based strain gradient theory for elasticity. Int. J. Solids Struct. **39**(10), 2731–2743 (2002)

Yang, Z., Cheng, D., Cong, G., Jin, D., Borjalilou, V.: Dual-phase-lag thermoelastic damping in nonlocal rectangular nanoplates. Waves Random Complex Media, 1–20 (2021)

Yang, S.T., Li, X.Y., Yu, T.L., Wang, J., Fang, H., Nie, F., et al., Zheng, L.M.: High-performance neuromorphic computing based on ferroelectric synapses with excellent conductance linearity and symmetry. Adv. Funct. Mater. **32**(35), 2202366 (2022). https://doi.org/10.1002/adfm.202202366

Yu, Y.J., Tian, X.G., Liu, J.: Size-dependent damping of a nanobeam using nonlocal thermoelasticity: extension of Zener, Lifshitz, and Roukes' damping model. Acta Mech. **228**, 1287–1302 (2017)

Yu, J.N., She, C., Xu, Y.P., Esmaeili, S.: On size-dependent generalized thermoelasticity of nanobeams. Waves Random Complex Media, 1–30 (2022)

Zeighampour, H., Beni, Y.T.: Cylindrical thin-shell model based on modified strain gradient theory. Int. J. Eng. Sci. **78**, 27–47 (2014)

Zener, C.: Internal friction in solids. I. Theory of internal friction in reeds. Phys. Rev. **52**(3), 230 (1937)

Zeng, H., Gao, N., Yin, Y., Zhang, M.: Recent progress in improving the performance of in vivo electrochemical microsensor based on materials. Curr. Opin. Electrochem. **33**, 100957 (2022)

Zhang, C.: The active rotary inertia driver system for flutter vibration control of bridges and various promising applications. Sci. China, Technol. Sci. **66**(2), 390–405 (2023). https://doi.org/10.1007/s11431-022-2228-0

Zhang, Z., Li, S.: Thermoelastic damping of functionally graded material micro-beam resonators based on the modified couple stress theory. Acta Mech. Solida Sin. **33**(4), 496–507 (2020)

Zhang, W., Kang, S., Liu, X., Lin, B., Huang, Y.: Experimental study of a composite beam externally bonded with a carbon fiber-reinforced plastic plate. J. Build. Eng. **71**, 106522 (2023). https://doi.org/10.1016/j.jobe.2023.106522

Zhao, C., Cheung, C.F., Xu, P.: High-efficiency sub-microscale uncertainty measurement method using pattern recognition. ISA Trans. **101**, 503–514 (2020). https://doi.org/10.1016/j.isatra.2020.01.038

Zhong, Q., Chen, Y., Zhu, B., Liao, S., Shi, K.: A temperature field reconstruction method based on acoustic thermometry. Measurement **200**, 111642 (2022)

Zhou, H., Li, P., Fang, Y.: Thermoelastic damping in circular cross-section micro/nanobeam resonators with single-phase-lag time. Int. J. Mech. Sci. **142**, 583–594 (2018)

Zuo, W., Li, P., Du, J., Tse, Z.T.H.: Thermoelastic damping in anisotropic piezoelectric microbeam resonators. Int. J. Heat Mass Transf. **199**, 123493 (2022)

Authors and Affiliations

Majid M. Kharnoob[1] · Lidia Castro Cepeda[2] · Edwin Jácome[2] · Santiago Choto[2] · Adeeb Abdulally Abdulhussien Alazbjee[3] · I.B. Sapaev[4,5] · Mohammed Ali Mahmood Hussein[6] · Yaicr Yacin[7] · Ahmed Hussien Radie Alawadi[8] · Ali Alsalamy[9]

✉ M.M. Kharnoob
  dr.majidkharnoob@coeng.uobaghdad.edu.iq

[1] Civil Engineering Department, University of Baghdad, Baghdad, Iraq

[2] Facultad de Mecánica, Escuela Superior Politécnica de Chimborazo (ESPOCH), Riobamba, Ecuador

[3] Collage of Medicine, Al-Ayen University, Thi-Qar, Iraq

[4] Tashkent Institute of Irrigation and Agricultural Mechanization Engineers, National Research University, Tashkent, Uzbekistan

[5] New Uzbekistan University, Tashkent, Uzbekistan

[6] Department of Refrigeration and Air Conditioning Technologies Engineering, Al Rafidain University College, Baghdad, Iraq

[7] Medical Technical College, Al-Farahidi University, Baghdad, Iraq

[8] Medical Laboratory Technology Department, College of Medical Technology, The Islamic University, Najaf, Iraq

[9] College of technical engineering, Imam Ja'afar Al-Sadiq University, Al-Muthanna 66002, Iraq